TT seminar on 25/10/2024

NICER analysis on millisecond pulsars

- **arXiv:2406.14466 →J0740+6620 (update of high-mass ms pulsar)**
- **arXiv:2407.06789 → J0437-4715 (nearest & brightest ms pulsar)**
- **arXiv:2409.14923 →J1231-1411 (complex case)**

Yudai Suwa (UTokyo, Komaba)

NICER and millisecond pulsars

- **NICERでこれまで観測したミリ秒パルサー**
- **https://arxiv.org/abs/1912.05705**
  - PSR J0030+0451（~1.4$M_\odot$）→ single
- **https://arxiv.org/abs/2105.06979**
  - PSR J0740+6620（~2.1$M_\odot$）→ binary
- **の2つ。今回新しく2つ追加。**

Models

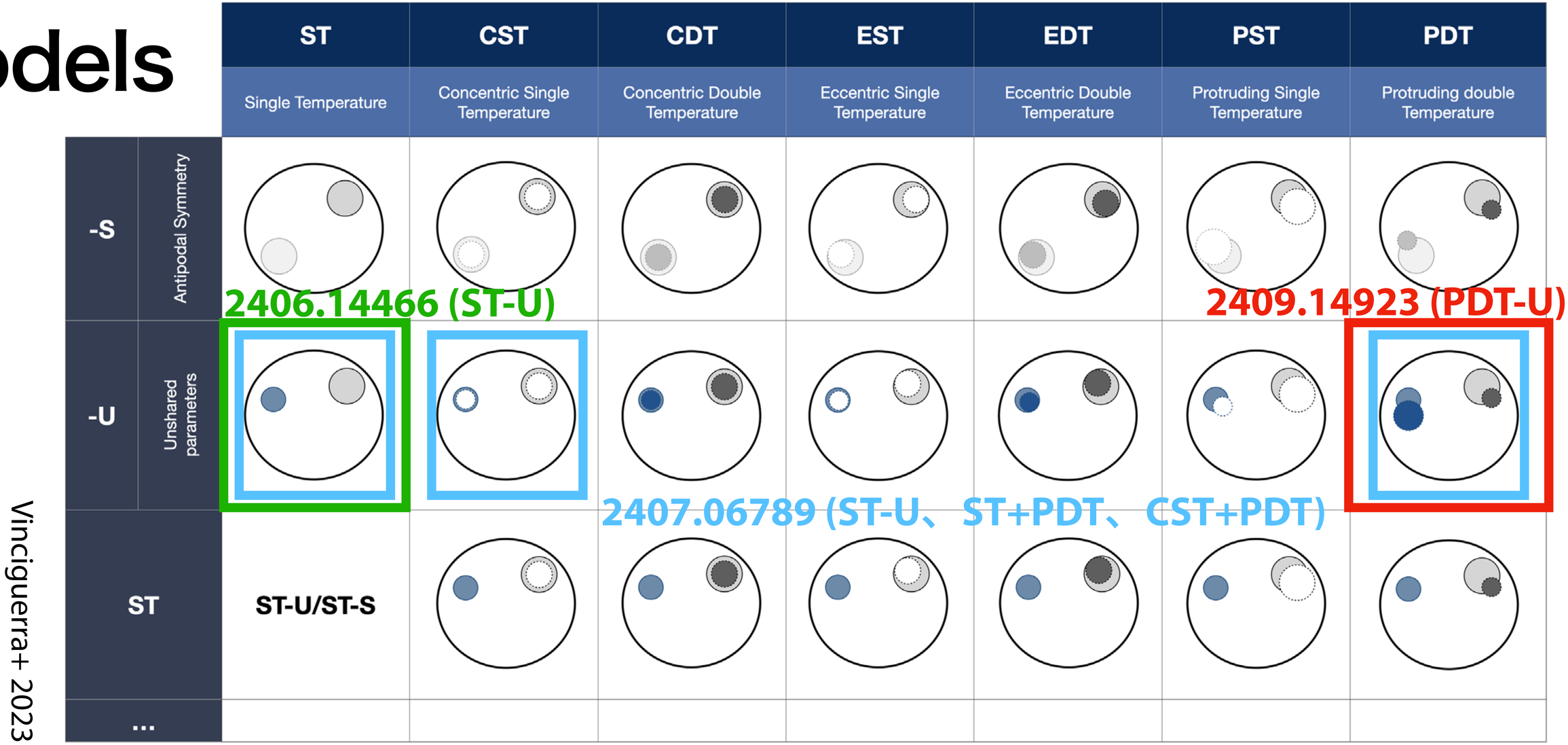

Figure 1. Schematic representation of naming convention adopted within X-PSI. Note that the protruding P configurations include the eccentric E ones, which, in turn, include the concentric ones C. In the case of antipodal symmetry (-S in the table), the lightest hot spot indicates that it is located on the hemisphere opposite to the observer. The dots in the last row of the table suggest how additional models could be built, allowing for different geometries for the two hot spots.

arXiv:2407.06789

Model explanation

- **ST-U:** The Single Temperature – Unshared (ST-U) model consists of two independent spherical caps with uniform effective temperature. The spot at the lower colatitude is the primary, and the parameters of each spot are independent.

- **ST+PDT:** In addition to the primary ST spot, there is a secondary Protruding Dual Temperature (PDT) spot with two overlapping spherical components. In the overlap, only one component's emission, called the superseding component, is considered.

- **CST+PDT:** In this model, the primary is a Concentric Single Temperature (CST) spot, made up of two spherical components: one emitting and one masking, forming a ring. The masking component, also called the omitting component (Vinciguerra et al. 2023, 2024), is concentric with the emitting one. The secondary spot is a PDT.

arXiv:2406.14466

PSR J0740+6620: basics

- **PSR J0740+6620**
- A high-mass pulsar
- Previously analyzed and updated with 3.6 yr of data from NICER and XMM-Newton
- $M > 2.0\ M_{\odot}$

arXiv:2406.14466

PSR J0740+6620: pulse profile

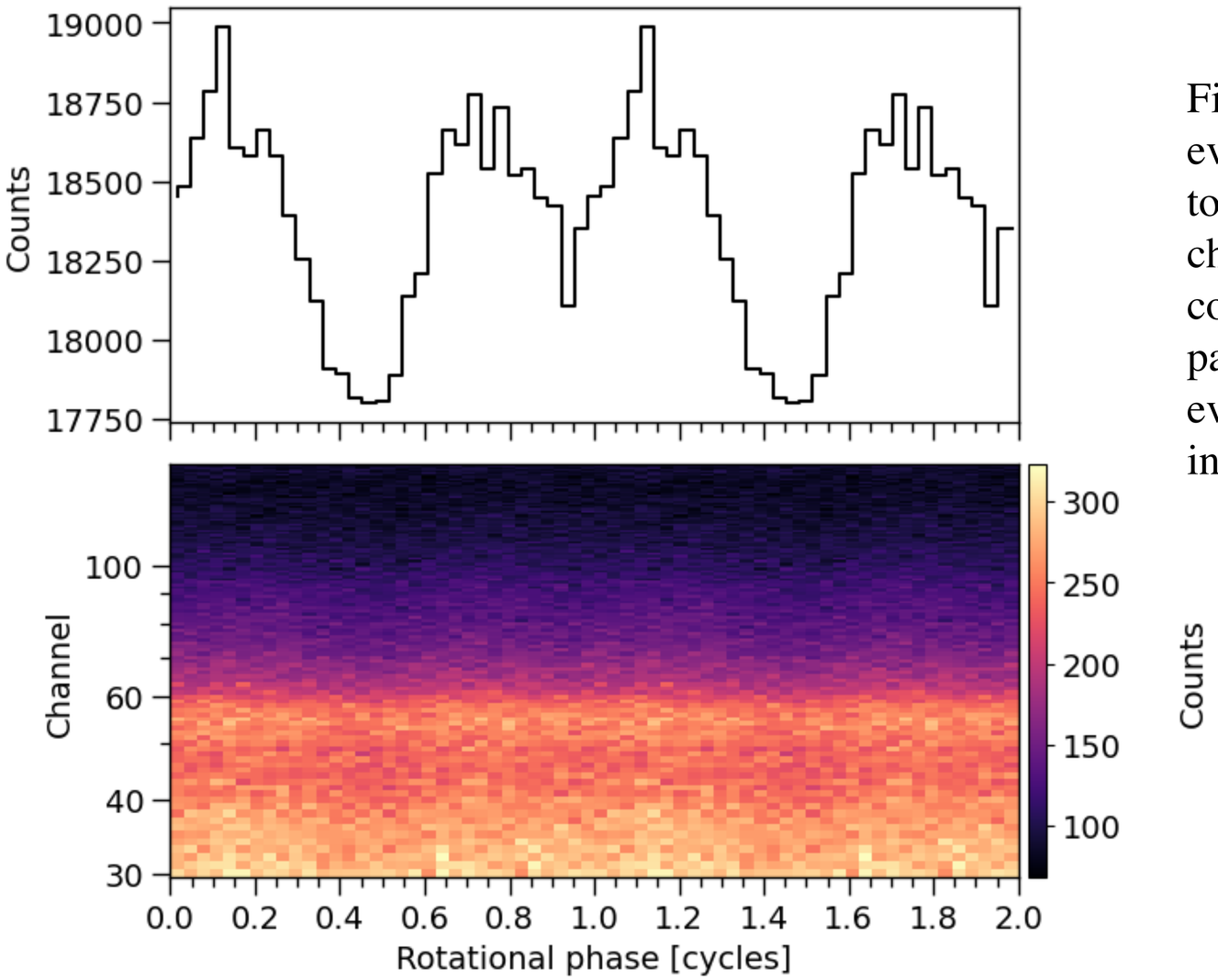

Figure 1. The new phase-folded PSR J0740+6620 event data for two rotational cycles (for clarity). The top panel shows the pulse profile summed over the channels. As in Figure 1 of R21, the total number of counts is given by the sum over all phase-channel pairs (over both cycles). For the modeling all the event data is grouped into a single rotational cycle instead.

PSR J0740+6620: M-R (new/old)

arXiv:2406.14466

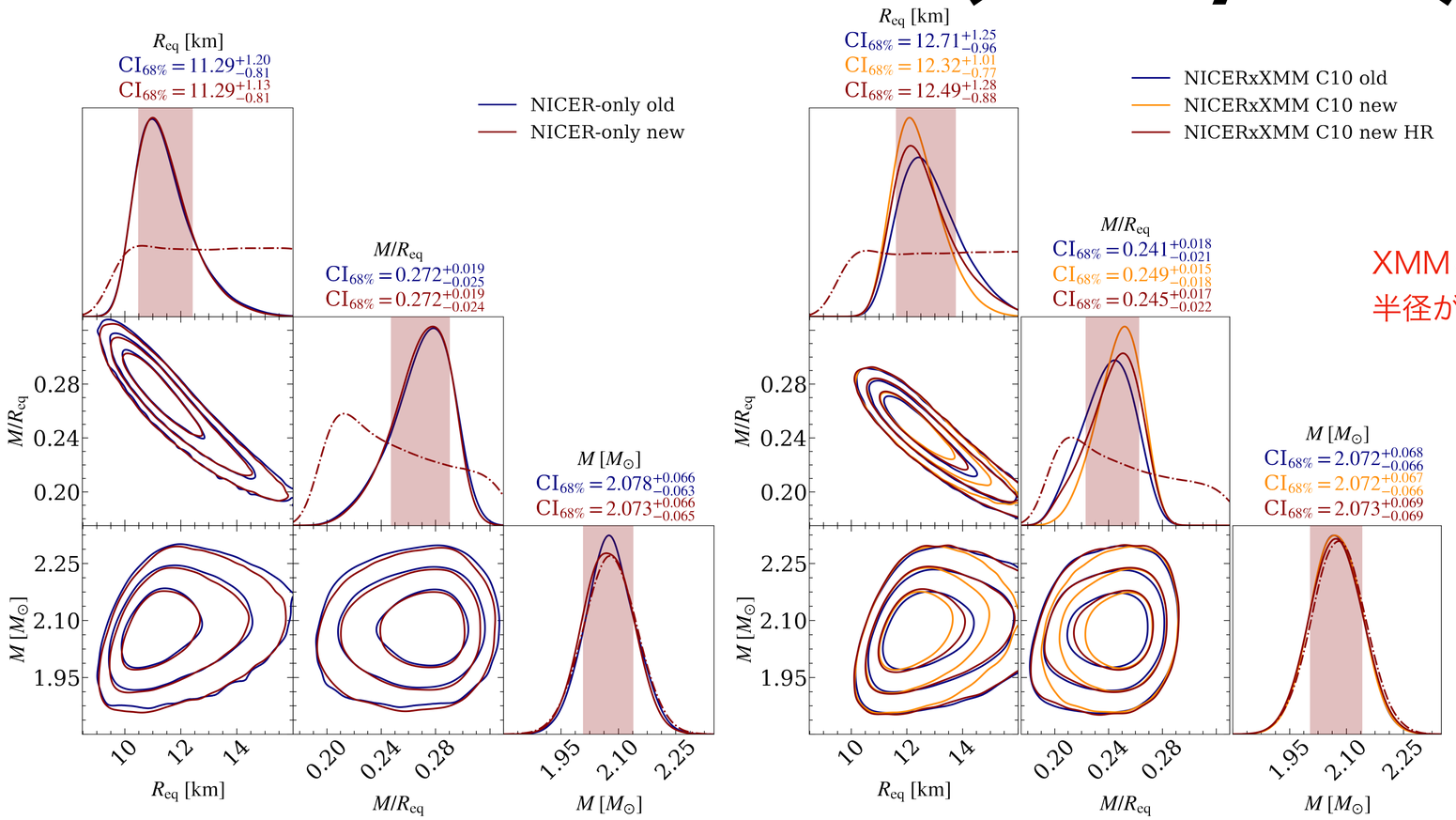

XMMと組み合わせるとシステマティックに半径が大きく見積もられる

Figure 2. Radius, compactness, and mass posterior distributions using the new NICER data set and ST-U model in the NICER-only analysis (left panel) and in the joint NICER and XMM-Newton analysis (right panel) compared to the old results from R21. Here "C10" refers to ±10.4 % calibration uncertainty in the overall effective area scaling factors, "new" and "old" without qualification have SE = 0.1 and "HR" refers to the new Headline Results with SE = 0.01. Dash-dotted functions represent the marginal prior probability density functions (PDFs). The shaded vertical bands show the 68.3% credible intervals (for the posteriors corresponding to the red curves), and the contours in the off-diagonal panels show the 68.3%, 95.4%, and 99.7% credible regions. See the captions of Figure 5 of S22 and Figure 5 of R21 for additional details about the figure elements.

arXiv:2406.14466

PSR J0740+6620: M-R (updated)

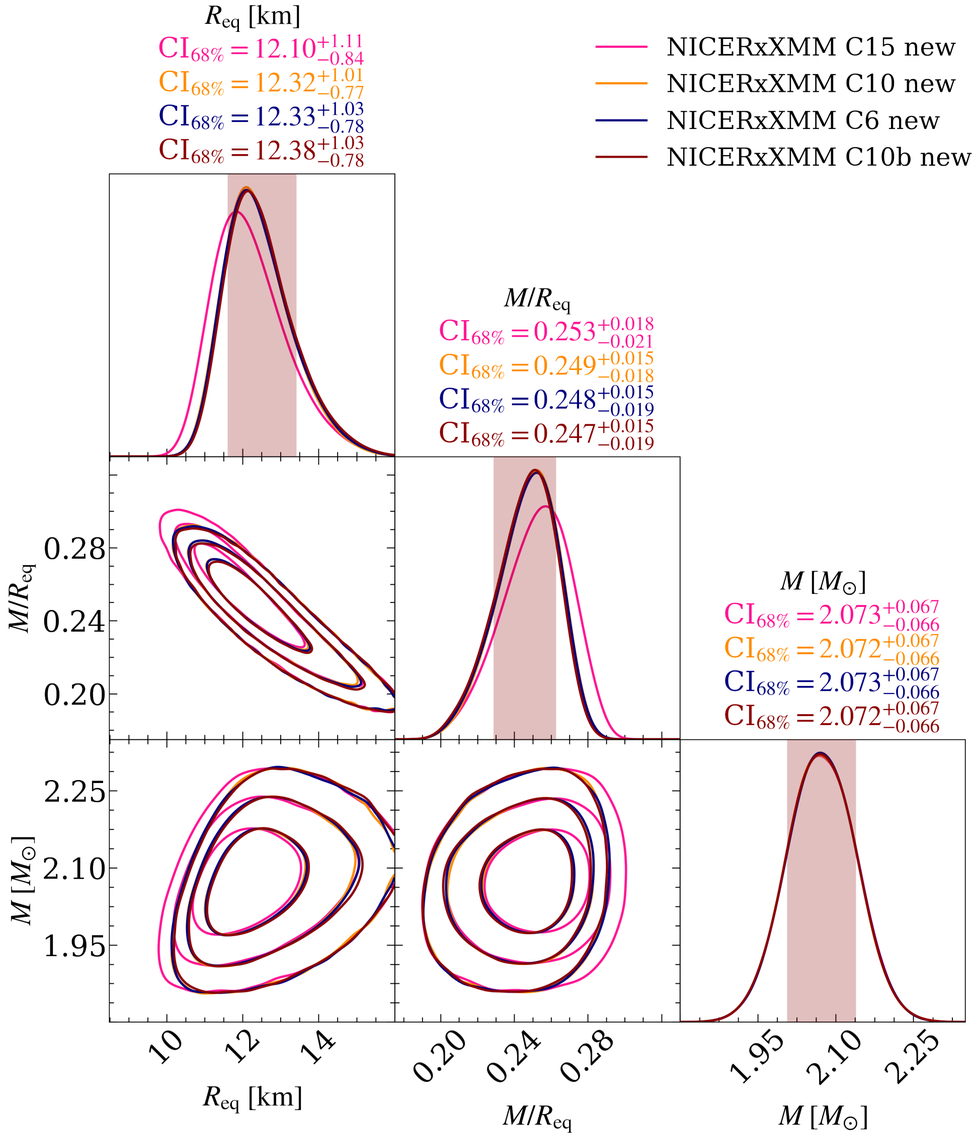

Figure 6. Posterior distributions for the space-time parameters using the new NICER data set and ST-U model in the joint NICER and XMM-Newton analyses, with different assumptions for the effective area scaling uncertainty and the used energy channels. Here “C15”, “C10”, “C6” refer to runs with ±15 %, ±10.4 %, and ±5.8 % uncertainties in the overall effective area scaling factors, respectively, and “C10b” to a run with ±10.4 % uncertainty and an alternative channel choice (see text at the end of Section 3.2). The contours for the three latter cases are almost exactly overlapping. See the caption of Figure 2 for additional details about the figure elements.

arXiv:2407.06789

PSR J0437-4715: basics

- **PSR J0437−4715**
- The nearest and brightest millisecond pulsar observed in X-rays
- A binary system with a 0.2 $M_\odot$ helium-core white dwarf
- Spin frequency of 174 Hz
- A well-constrained distance of 156.98 ± 0.15 pc
- Shapiro delay provides independent mass constraints: 1.418 ± 0.044 $M_\odot$

arXiv:2407.06789

PSR J0437-4715: pulse profile

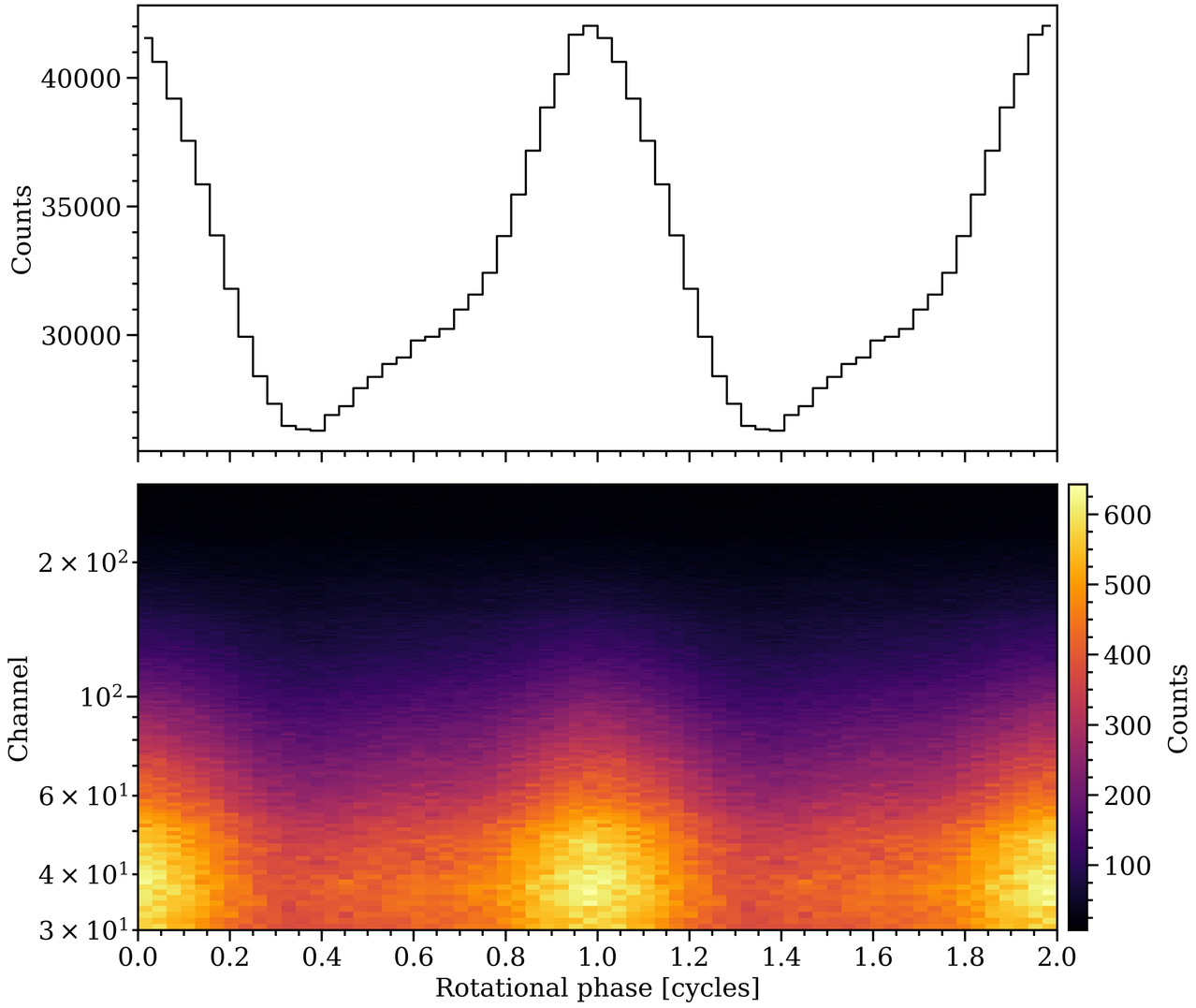

Figure 1. Phase-folded PSR J0437−4715 (3C50) event data shown over two rotational cycles. We use 32 phase intervals (bins) per cycle and the count numbers in bins separated by one cycle are identical for a given channel(s). The sum over all phase-channel pairs yields the total counts. The top panel displays the waveform obtained by summing the channels in the contiguous subset [30, 300). The bottom panel displays the phase-channel-resolved count numbers for the same channel subset, where the color bar represents counts per channel per two cycles.

PSR J0437-4715: M-R

arXiv:2407.06789

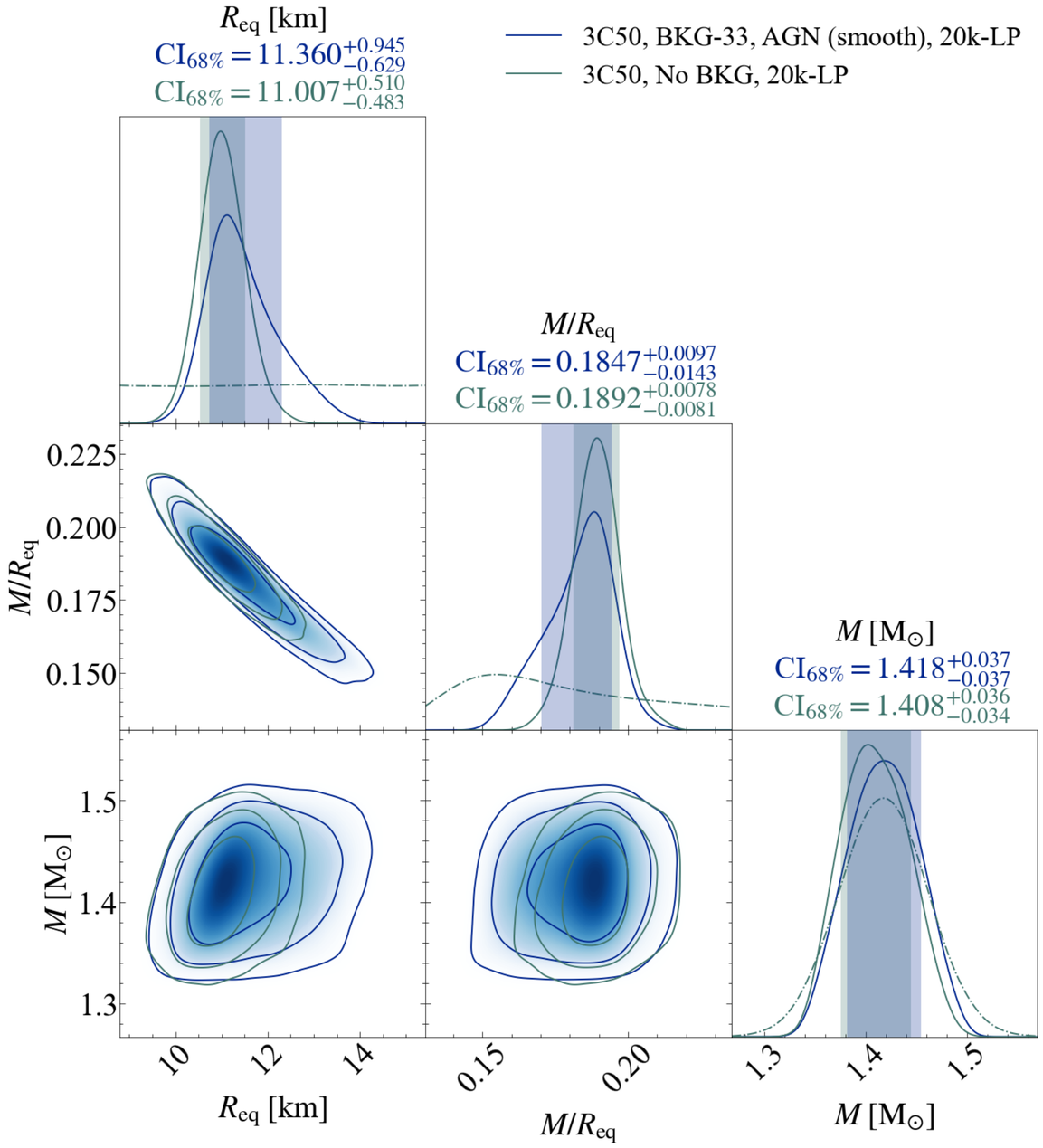

Figure 8. Mass, radius and compactness posteriors inferred by the high MultiNest resolution CST+PDT runs, both in the absence of any background constraints, and in the presence of lower and upper background constraints involving the instrument background and 3C50 AGN spectrum. The 2-D marginalized posteriors of the latter model, that constitutes our headline result, are shaded in blue. Both runs infer highly consistent radius posteriors, with the background-constrained run consisting of a distribution tail that extends slightly more towards higher radii.

arXiv:2407.06789

PSR J0437-4715: M-R

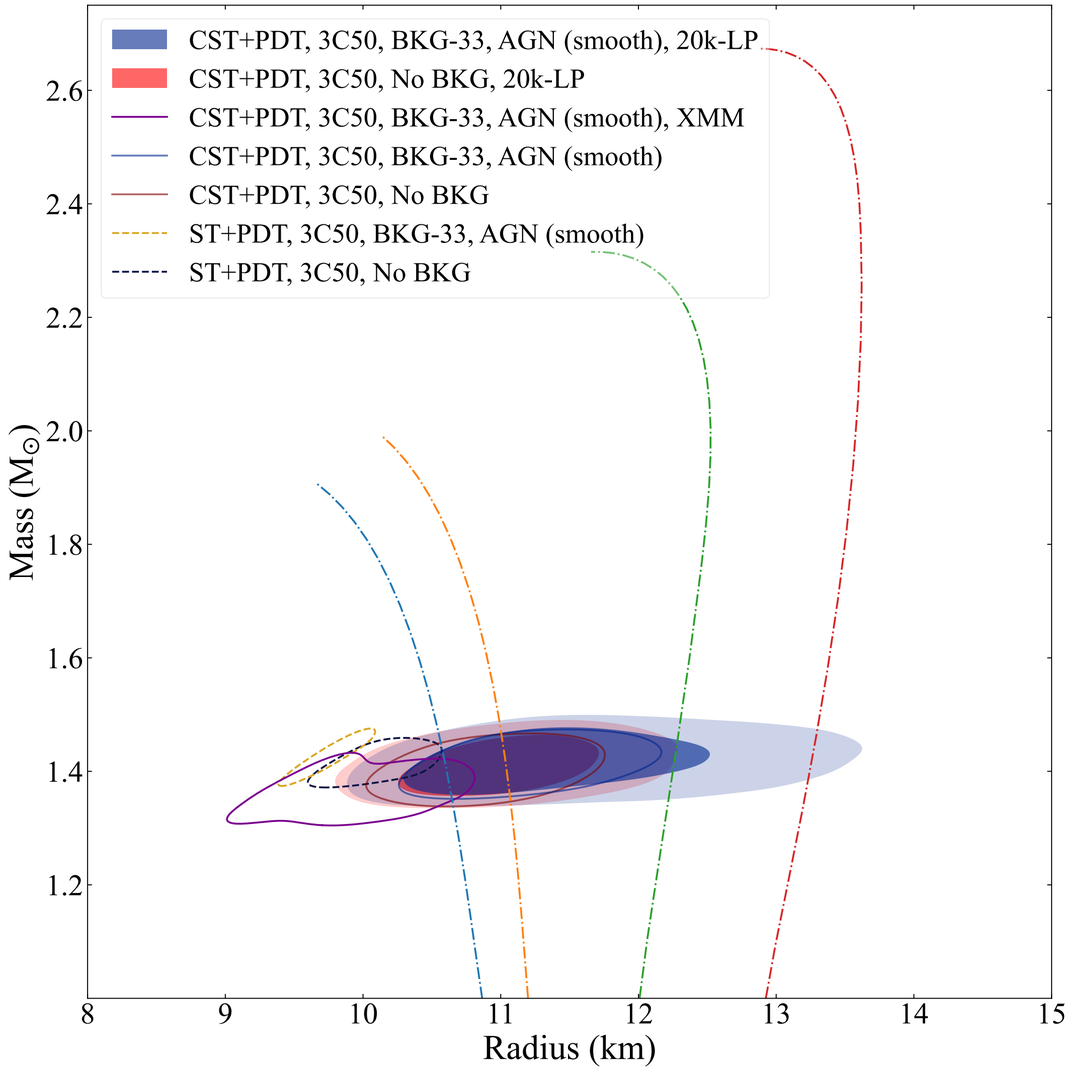

Figure 16. Inferred mass and radius posteriors for the different capable models explored in this paper, compared to mass-radius curves from EoS models. The shaded contours are the 68% and 95% credible regions for the high-res CST+PDT runs, and the remaining contours represent the 68% credible regions for the default resolution CST+PDT and ST+PDT runs. The colored dash-dot lines are example mass-radius curves generated using one of the families of EoS models explored in Rutherford et al. (2024). It employs the Baym-Pethick-Sutherland crust EoS (Baym et al. 1971) at densities less than 0.5 times the nuclear saturation density n_S; the N^{3}LO χEFT band from Keller et al. (2023) at densities 0.5-1.5 n_S; and a parametrized piecewise polytropic (PP) model (Hebeler et al. 2013) at higher densities. The parameters for the mass-radius relations shown here have been chosen to span the range of stiffness allowed by this model that is also compatible with the existence of $\sim 2.0\ M_\odot$ neutron stars.

arXiv:2409.14923

PSR J1231-1411: basics

- **PSR J1231-1411**
- A rotation-powered millisecond pulsar in a binary system
- Spin frequency of 271 Hz
- It's surface regions are thermally emitting, likely heated by magnetospheric return currents

arXiv:2409.14923

PSR J1231-1411: pulse profile

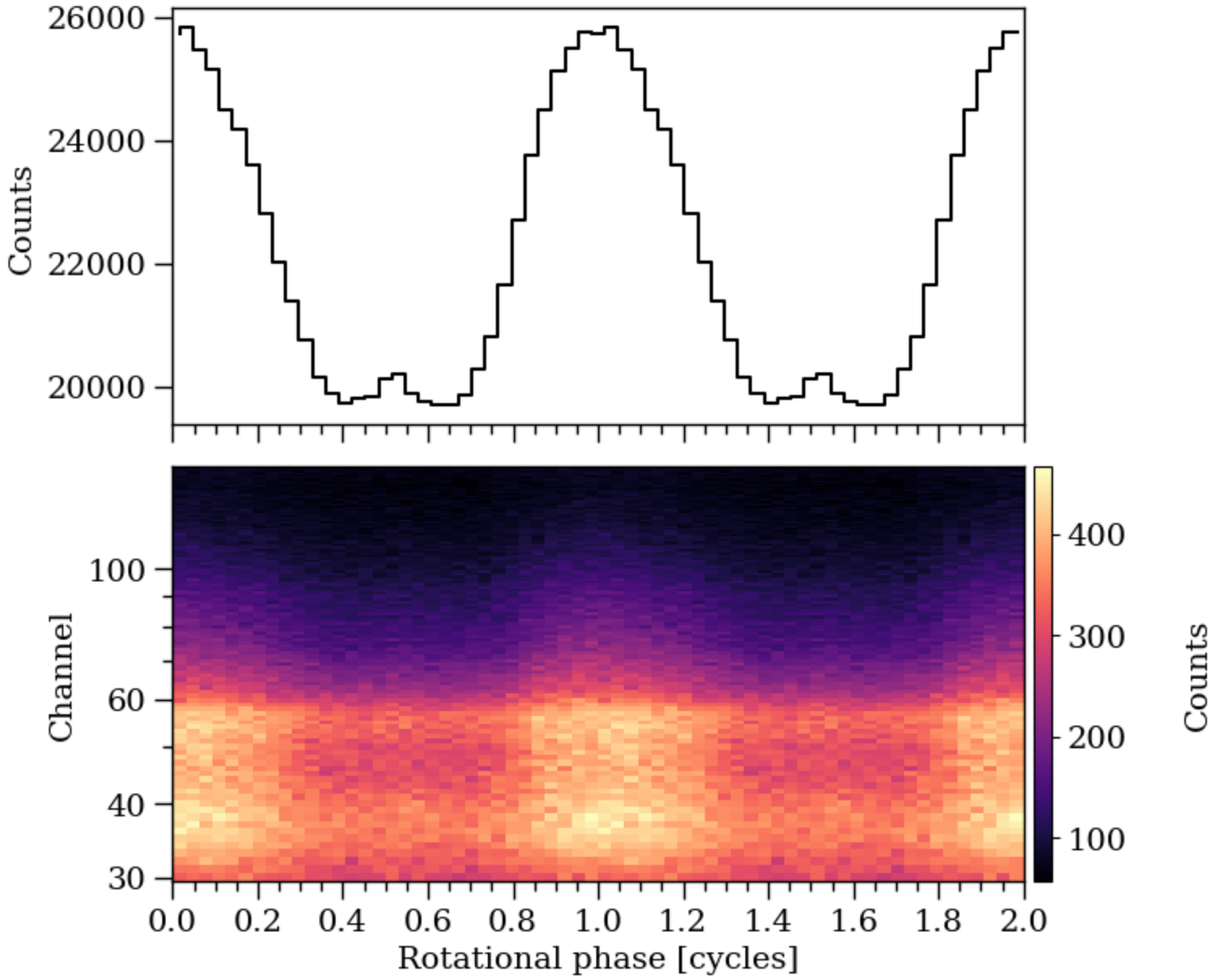

Figure 1. The phase-folded PSR J1231−1411 event data for two rotational cycles (for clarity). The top panel shows the pulse profile summed over the channels. The total num- ber of counts is given by the sum over all phase-channel pairs (over both cycles). For the modeling all the event data are grouped into a single rotational cycle instead, and thus each phase-channel bin has twice the number of counts shown here.

PSR J1231-1411: M-R

arXiv:2409.14923

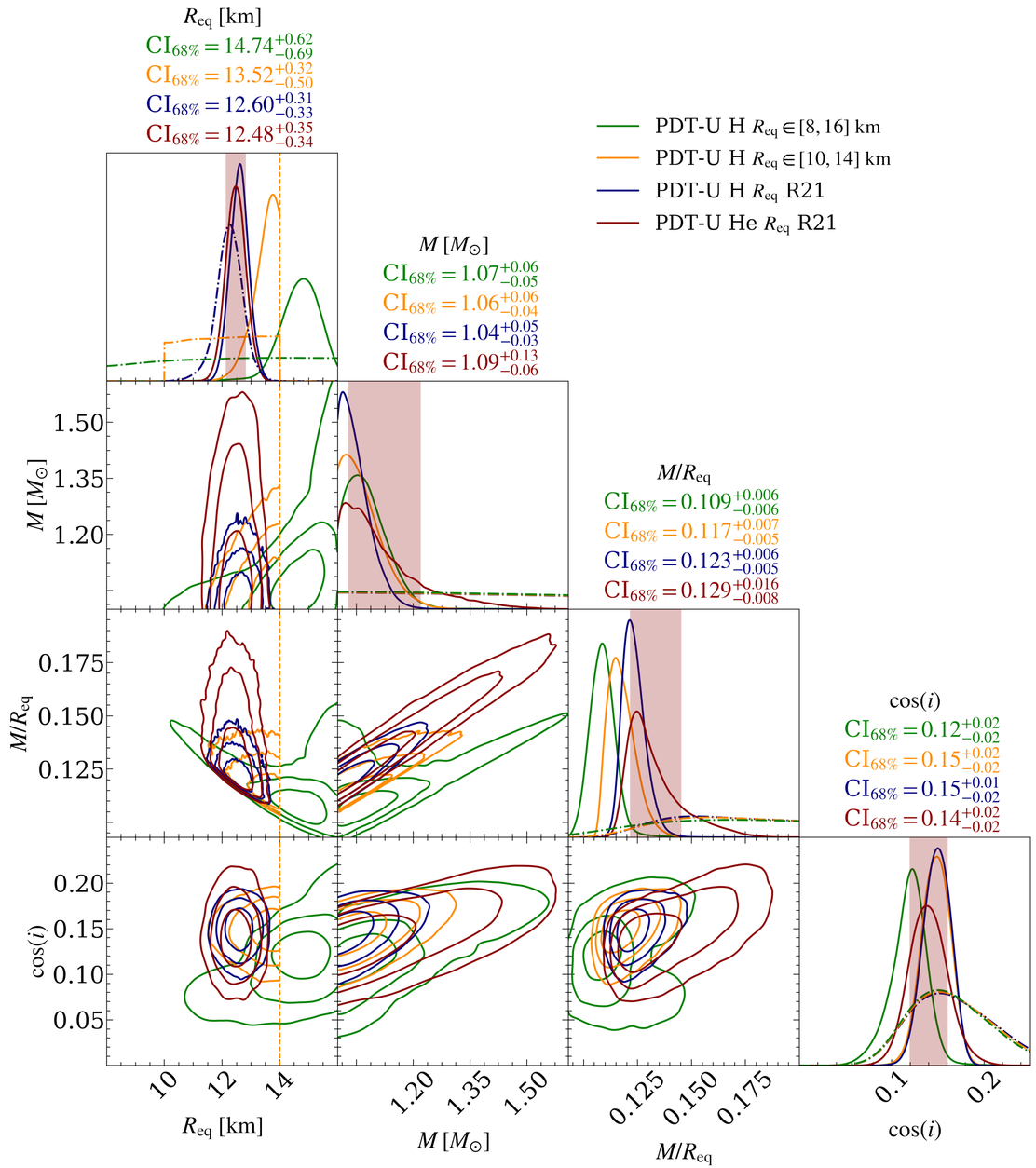

Figure 5. Radius, mass, compactness and inclination posterior distributions using the NICER and XMM-Newton data sets for the PDT-U model. The results with three different radius priors are shown, but the run with widest radius prior (Req ∈ [8, 16] km) seems not converged as it finds only significantly worse fits to the data than the others. Dash-dotted curves represent the marginal prior probability density functions (PDFs). The vertical dashed orange line shows Req = 14 km to guide the eye. The shaded vertical bands show the 68.3% credible intervals (for the posteriors corresponding to the red curves), and the contours in the off-diagonal panels show the 68.3%, 95.4%, and 99.7% credible regions. See the captions of Figure 5 of Riley et al. (2021) for additional details about the figure elements.

これは推定できていると言えるのか。。。？

Summary of M-R

- **PSR J0740+6620 (update of high-mass ms pulsar)**
  - $M = 2.073^{+0.069}_{-0.069}\, M_\odot$
  - $R = 12.49^{+1.28}_{-0.88}\,\mathrm{km}$
- **PSR J0437-4715 (nearest & brightest ms pulsar)**
  - $M = 1.418^{+0.037}_{-0.037}\, M_\odot$
  - $R = 11.36^{+0.95}_{-0.63}\,\mathrm{km}$
- **PSR J1231-1411 (complex case)**
  - $M = 1.04^{+0.05}_{-0.03}\, M_\odot$ (!?)
  - $R = 12.6^{+0.3}_{-0.3}\,\mathrm{km}$

Sotani, Nishimura, Naito (2022)